nature materials

Supplementary Information for

Pen-drawn Marangoni swimmer

Seo Woo Song†*, Sumin Lee†, Jun Kyu Choe, Amos Chungwon Lee, Junwon Kang, Gyeongjun Kim, Huiran Yeom, Yeongjae Choi, Sunghoon Kwon*, Jiyun Kim*

†These authors contributed equally to this work.
*Correspondence to: seowoo313@snu.ac.kr, skwon@snu.ac.kr, jiyunkim@unist.ac.kr

The PDF file includes:

Supplementary Text
Figs. S1 to S4
Captions for movies S1 to S9

Other Supplementary Information for this manuscript include the following:

Movies S1 to S9 (.mp4)

Supplementary Text

Finite element analysis simulation modeling

Commercially available finite element analysis (FEA) software, ABAQUS, was used to predict the trajectories of the swimmers. To derive the driving pressure, we first calculated the friction coefficient μ (3.327 10^{-5} $Nm^{-1}s$) from the relaxation of the swimmers by using the following equation:

$$v(t) = v_{init}\, e^{-\frac{\mu}{m}t},$$

where m is the mass of the boat (0.07 g) and v_{init} is the initial velocity of the swimmer. Then, we calculated the driving force F_0 of each sample of camphor ink of different concentrations from their steady-state velocity v_{steady} using the following equation:

$$F_0 = \mu v_{steady}\sqrt{\frac{v_{steady}^2}{4kD} + 1}\,,$$

where k is the relaxation rate and D is the effective diffusion coefficient. Because these constants are broadly applicable to a variety of situations regardless of the shape of the swimmer, we used the values k = 2 10^{-2} s^{-1} and D = 4 10^{-3} m^2s^{-1} adopted from a previous report *(N. J. Suematsu et al.*, *Langmuir* 2014). The driving pressure was then calculated for each concentration by dividing the driving force by the working area (the side area of the swimmer where the camphor ink was drawn, A = 3 mm^2). For the camphor inks applied in dots, we analyzed the diameter of the dots and applied the driving pressure to the swimmer at the appropriate locations with equivalent ratios. Finally, stagnation pressure P_s was applied to the sides of the swimmer, as computed by the following equation:

$$P_s = -c_s\left(v \cdot n - v_{ref} \cdot n\right)^2,$$

where c_s is the fitted coefficient (c_s = 1.4 kg/m^3), n is the normal unit outward from the element where the surface pressure is applied, and v_{ref} is the velocity of the reference node.

In all simulations, the swimmers were constructed with 3D deformable solid elements of type C3D8 using a linear elastic model. The mechanical properties were determined by using the following input parameters: density d = 1.45 g/cm^3, Young's modulus E = 3.275 GPa, and Poisson's ratio v = 0.4.

Theoretical analysis of camphor-based Marangoni swimmer

Marangoni propulsion is driven by the surface tension gradient induced by camphor release. Therefore, the mathematical model of camphor can be established using the two differential equations—Newtonian equation and reaction–diffusion equation. When neglecting the spatial gradient created by the camphor molecules and bulk concentration of the camphor molecules on the water surface, the mean surface concentration of the camphor can be calculated by solving the differential equation of the mean surface concentration described in equation (3).

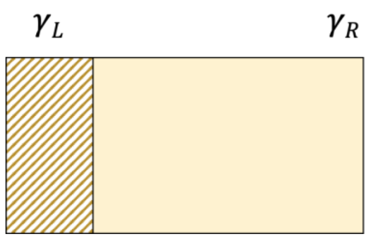

$\frac{d\gamma}{dx}$: **Marangoni propulsion (Driving force)**

$\Delta\gamma = \gamma_R - \gamma_L$

Reaction–diffusion equation:

$$\frac{\partial\Gamma(x,t)}{\partial t} = D\nabla^2\Gamma(x,t) - \kappa\Gamma(x,t) + \alpha L^{-1}\delta(x - x_0) \qquad (1)$$

Newtonian equation:

$$M\frac{d^2x}{dt^2} = -\mu\frac{dx}{dt} + F_w = 0 \qquad (2)$$

$$F_w = w(r_0 - r(\Gamma(x,t))$$

Equation for mean surface concentration of camphor:

$$\frac{d\Gamma(t)}{dt} = -k\Gamma(t) + \frac{\alpha(p)}{A} \qquad (3)$$

Parameters:

A	supply rate of camphor molecules	[mol s^{-1}]
*F*w0	driving force of the stationary camphor boat	[N]
m	mass of the camphor boat (= 20 × 10^{-6})	[kg]

x_0	position at the edge of the camphor disk	[m]
μ	friction coefficient	[N m^{-1} s]
F_w	driving force of the moving camphor boat	[N]
γ	surface tension	[N m^{-1}]
γ_0	surface tension of pure water	[N m^{-1}]
Γ	surface camphor concentration	[mol m^{-2}]
D	effective diffusion coefficient	[m^2 s^{-1}]
k	sum of k_s and k_d	[s^{-1}]
k_s	sublimation rate from the water surface	[s^{-1}]
k_d	dissolution rate from the water surface	[s^{-1}]
L	length of the contact line between the camphor disk and water surface	[m]
α (p)	supply rate of camphor molecules from the disk to the water surface depending on the position p of attachment of the camphor disk to the plastic plate	[mol s^{-1}]
A	surface area of the water phase	[m^2]

Theoretical analysis of camphor trajectory according to design of camphor engine

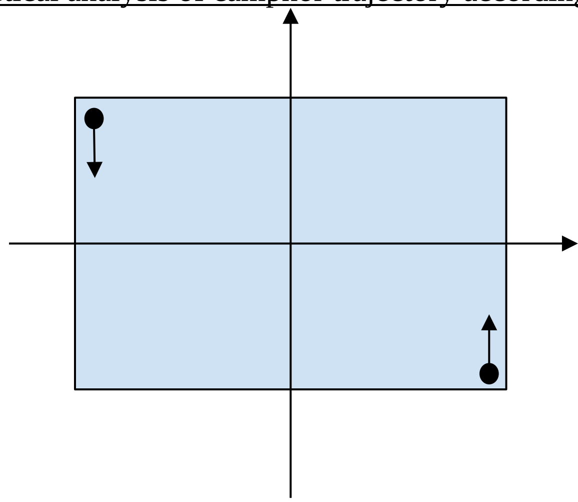

(M: mass of swimmer, a: width of swimmer, b: length of swimmer, I: Inertial moment, ν: velocity of rigid body, Fw: Driving force of camphor boat, F = $Fw - \mu v$).

We placed two camphor engines on both vertices of a rectangular Marangoni swimmer. Assuming that the Marangoni swimmer is a rigid body and two points are considered, the system can be interpreted as a mathematical model using the kinematics with Newtonian, net torque, and reaction–diffusion equations. We can easily derive equations (2) and (3) for the net force equation by definition.

Reaction–diffusion equation:

$$\frac{\partial \Gamma(x,t)}{\partial t} = D\nabla^2\Gamma(x,t) - \kappa\Gamma(x,t) + \alpha L^{-1}\delta(x - x_0) \quad (1)$$

Net force - Newton's equation:

$$M\frac{d^2x}{dt^2} = -\mu\frac{dx}{dt} + F_w = 0 \quad (2)$$

$$F_w = w(r_0 - r(\Gamma(x,t)) \quad (3)$$

Equation (4) can be established using the equation $\Sigma\tau = r \times F$ and the moment of inertia of the rectangle. Equation (5) is derived by utilizing the equation $\nu = r\frac{d\theta}{dt}$ and moment of inertia. We assume that the diffusion rate of camphor molecules is faster than the spatial gradient, which can be neglected, and that the water surface area is large enough to neglect the concentration of the released camphor molecules. Then, we can derive equation (7), which leads to a differential equation with only one variable of θ. Therefore, mathematical modeling can easily explain the behavior of the Marangoni swimmers.

Net Torque:

Moment of inertia: $I = \frac{1}{12}M(a^2 + b^2)$

$$I\,\frac{d^2\theta}{dt^2} = (F_w - \mu v)\,\frac{a}{2} + (F_w - \mu v)\,\frac{a}{2} = (F_w - \mu v)a \tag{4}$$

$$(v = \frac{\sqrt{a^2 + b^2}}{2}\frac{d\Theta}{dt})$$

$$\frac{1}{12}M(a^2 + b^2)\,\frac{d^2\theta}{dt^2} = (F_w \cdot a - \mu\,\frac{\sqrt{a^2+b^2}}{2}\frac{d\Theta}{dt} \cdot a) \tag{5}$$

$$\frac{1}{12}M(a^2 + b^2)\,\frac{d^2\theta}{dt^2} = (a^2(r_0 - r\Gamma(x,t)) - \mu\,\frac{\sqrt{a^2+b^2}}{2}\frac{d\Theta}{dt} \cdot a) \tag{6}$$

$$\frac{1}{12}M(a^2 + b^2)\,\frac{d^2\theta}{dt^2} = a^2(r_0 - r\,\frac{\alpha(p)RT}{kA}(1 - e^{-kt})) - \mu\,\frac{\sqrt{a^2+b^2}}{2}\frac{d\Theta}{dt} \cdot a \tag{7}$$

Supplementary Figures

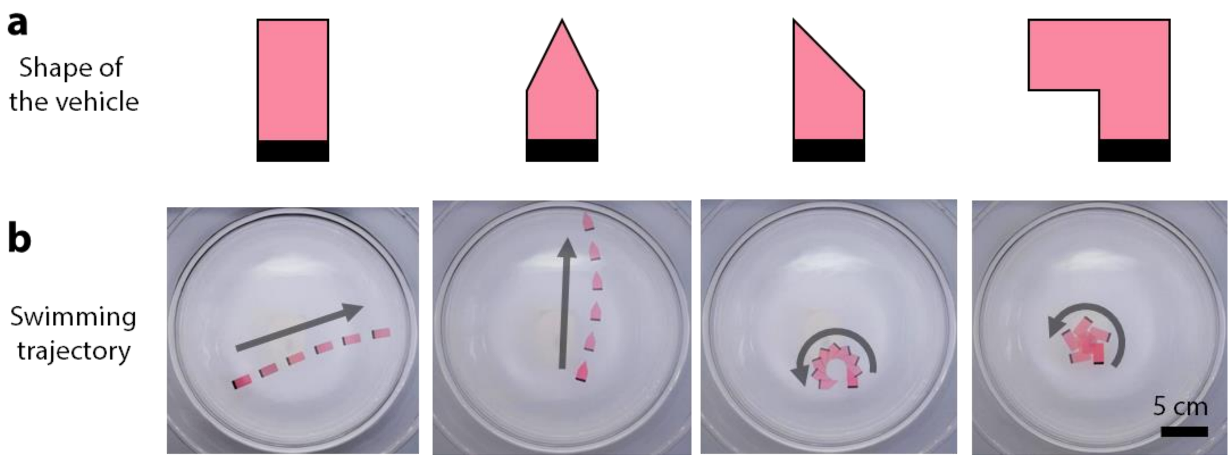

fig. S1. Swimming trajectories according to the shape of the vehicle. a, Marangoni swimmers with different shapes of the vehicle. The swimmers in this experiment have vehicles of different shapes but the same pattern of the camphor engine. **b,** Trajectories of the swimmers with vehicles of different shapes.

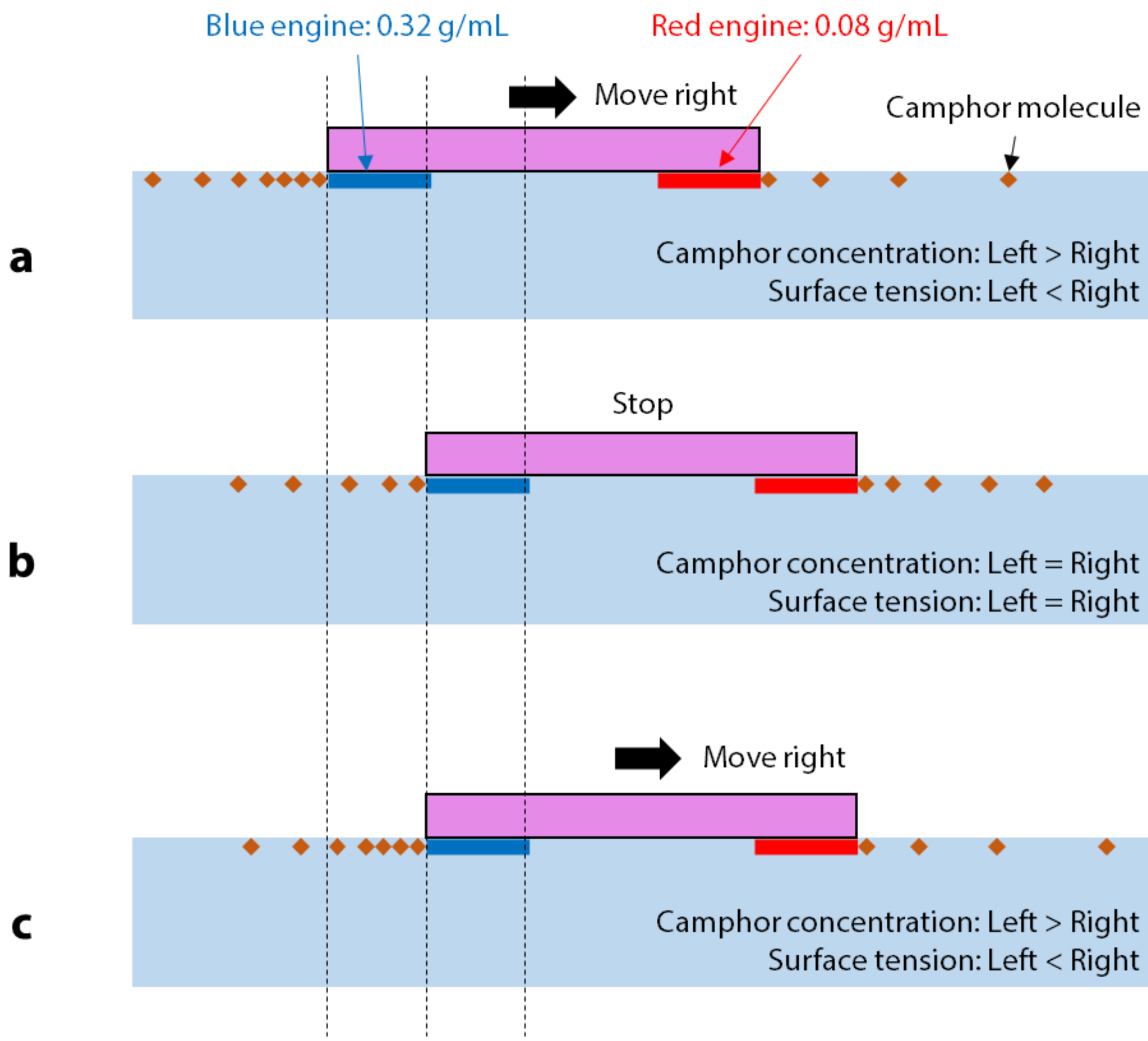

fig. S2. Theoretical model of intermittent movement of an asymmetric Marangoni swimmer. **a,** A blue camphor engine drawn with higher camphor concentration releases the camphor molecules more rapidly. Because camphor concentration on the left side is higher than that on the right side, the swimmer moves toward the right. **b,** The camphor molecules on the right side are compressed and those on the left side are dispersed as the swimmer moves to the right. Hence, the camphor concentrations on both sides become equal and the swimmer stops. **c,** As the swimmer releases the camphor in place, an imbalance between the camphor concentrations on both sides occurs again and the swimmer moves.

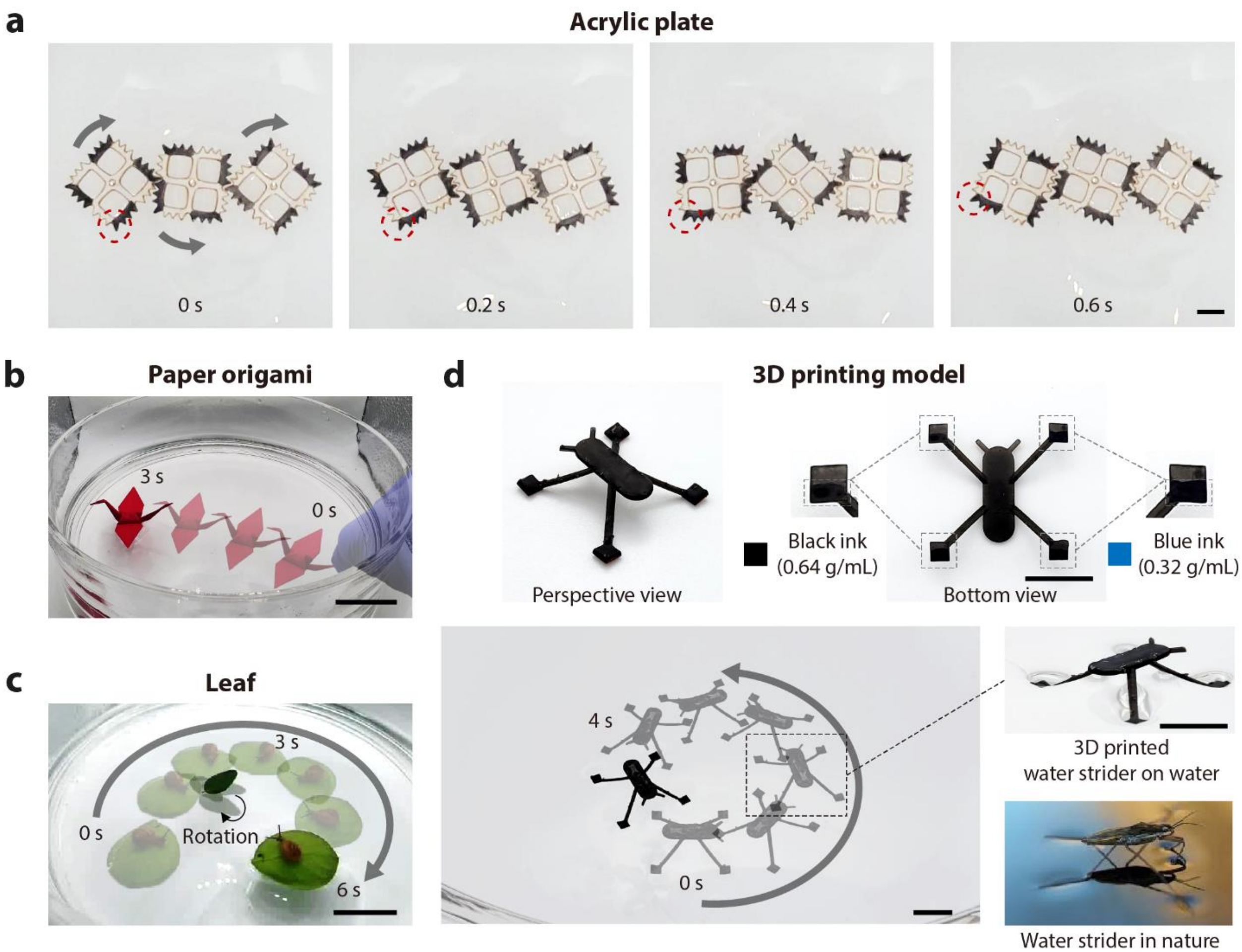

fig. S3. Versatile applicability of pen-drawn Marangoni swimmers on various substrates. The pen-based approach allows the fabrication of Marangoni swimmers with various substrates: **a,** acrylic plate, **b,** paper origami, **c,** natural surfaces like leaves, and **d,** 3D printed structures. Scale bars: 1 cm (a and d), 5 cm (b), and 3 cm (c). See also movie S6.

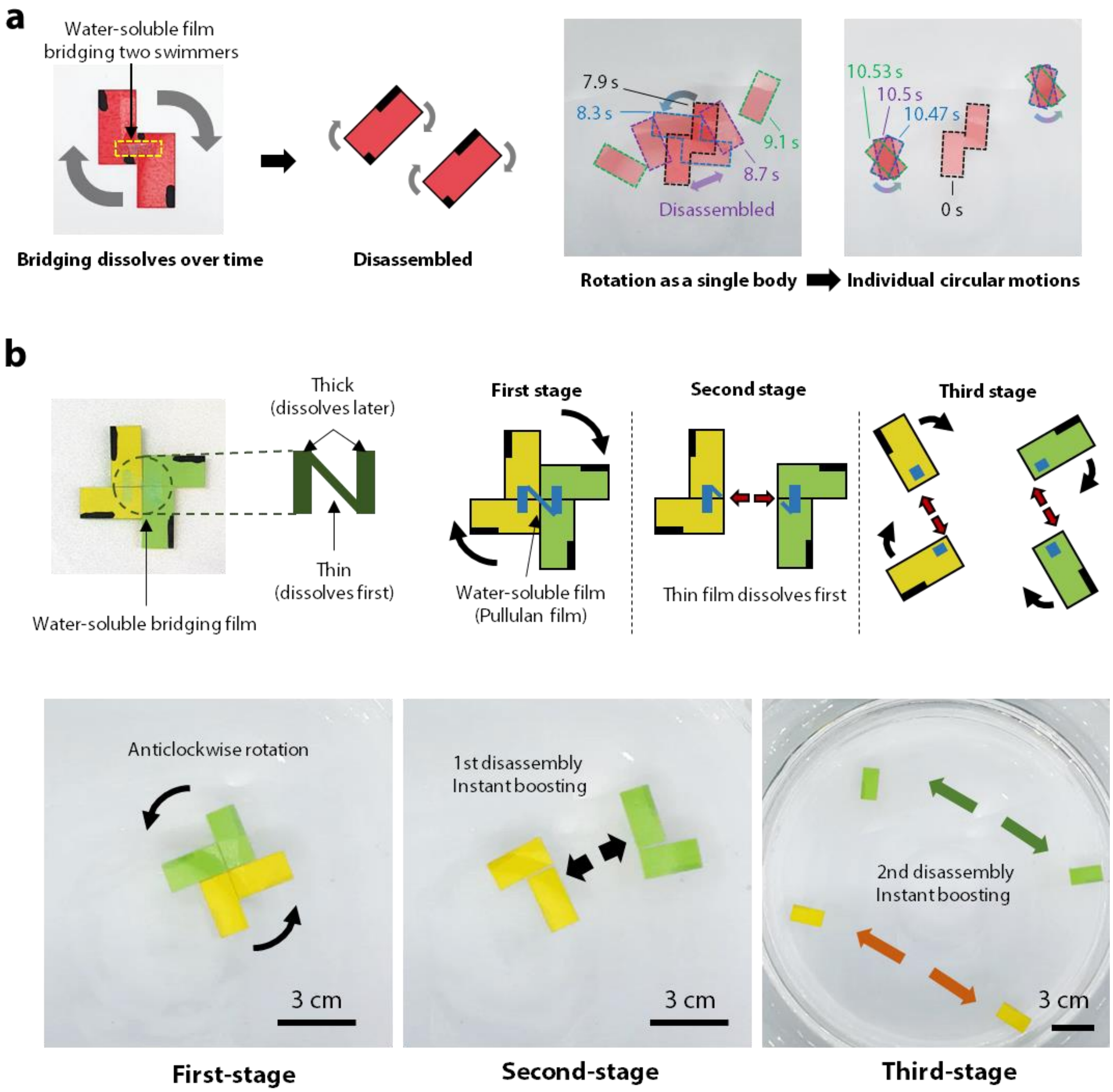

fig. S4. Multistep motion programming using water-soluble bridges. a, Two-step motion programming. **b,** Three-step motion programming.

Movie S1. Overview of pen-drawn Marangoni swimmers
This movie presents the experimental results and fabrication process of robots shown in Fig. 1b-d. Pen-drawn Marangoni swimmers, capable of complex locomotion, can be prepared within 10 s. The versatile applicability of the pen-based approach facilitates the integration of a pen-drawn-camphor engine with various substrates, including 3D structures. Integration with time-varying substrates allows multistep motion programming.

Movie S2. Quantitative analysis of swimmers' speed using ImageJ
'Mosaic' plugin in ImageJ was used for quantitative analysis of the swimmers' speed.

Movie S3. Controllable motion of pen-drawing Marangoni swimmer
This movie presents the results of the experiments and simulations shown in Fig. 2e and f. The time interval between successive frames in Fig. 2e and f is 0.33 s.

Movie S4. Complex motion programming by combining different functional modules
This movie presents the results of the experiments shown in Fig. 3a and b. The programming of a star-shaped trajectory and square trajectory is demonstrated.

Movie S5. Practical applications of functional module combination for complex motion programming
This movie presents the results of the experiments shown in Fig. 4. The programming of a pathfinding swimmer and a robot soccer player is demonstrated.

Movie S6. Versatile applicability of pen-drawn Marangoni swimmer on various substrates
This movie presents the results of the experiments shown in fig. S3. The applications of a pen-drawn camphor engine on an acrylic plate, paper origami, leaf, and 3D printed structures are demonstrated.

Movie S7. Multiple leaf swimmers
Fabrication of pen-drawn Marangoni swimmers on leaves is demonstrated. Each leaf swimmer rotates clockwise or anticlockwise depending on the camphor engine pattern. The swimmers tend to maintain a distance between themselves owing to the decreased surface tension around each swimmer.

Movie S8. Multistep motion programming with paper as a time-dependent transformable substrate
This movie presents the results of the experiments shown in Fig. 5. Three different swimming modes of a rocket-shaped swimmer, depending on the engine arrangement, were demonstrated. As the folded region contacts the water surface over time, the activated second-stage engine changes the motion of the swimmer.

Movie S9. Multistep motion programming using water-soluble bridges and its application to cargo delivery
This movie presents the results of the experiments shown in Fig. 6. The water-soluble bridging film enables the disassembly of swimmers in a time-dependent manner in addition to multistep motion programming. A swimmer capable of delivering cargo to the target location and returning to the original location is demonstrated by using this property.